ARTICLES
https://doi.org/10.1038/s41566-019-0449-8
nature photonics

Self-organized nonlinear gratings for ultrafast nanophotonics

Daniel D. Hickstein[1*], David R. Carlson[1], Haridas Mundoor[2], Jacob B. Khurgin[3], Kartik Srinivasan[4], Daron Westly[4], Abijith Kowligy[1], Ivan I. Smalyukh[2,5,6], Scott A. Diddams[1,7] and Scott B. Papp[1,7*]

As devices utilizing femtosecond-duration laser pulses become more commonplace, there is a need for next-generation nonlinear-photonics technologies that enable low-energy femtosecond pulses to be converted from one wavelength to another with high efficiency. However, designing nonlinear materials to operate with femtosecond pulses is challenging, because it is necessary to match both the phase velocities and group velocities of the light. Here, we show that femtosecond laser pulses can generate self-organized nonlinear gratings in nanophotonic waveguides, thereby providing a nonlinear optical device with both quasi-phase-matching and group-velocity matching for second-harmonic generation. We use nonlinear microscopy to uniquely characterize the self-organized nonlinear gratings and demonstrate that these waveguides enable simultaneous $\chi^{(2)}$ and $\chi^{(3)}$ nonlinear processes for laser-frequency-comb stabilization. Finally, we derive the equations that govern self-organized grating formation for femtosecond pulses and uncover the crucial role of group-velocity matching. In the future, nanophotonics with self-organized gratings could enable scalable, reconfigurable nonlinear photonics.

Nonlinear light–matter interactions can convert photons to new frequencies and serve as fundamental tools for laser science[1], telecommunication[2], quantum computation[3] and other disciplines across science and technology[4]. As these applications become increasingly widespread, there is a need for nonlinear-optical platforms that are small, adaptable, easy to fabricate, low cost and efficient. Achieving high conversion efficiency requires matching the phase velocities of each wavelength of light used in the nonlinear interaction. In some cases, a fortuitous material birefringence can provide a mechanism for this phase-velocity matching, but in many cases quasi-phase-matching (QPM) is the preferred option. QPM typically involves periodically flipping the direction of the nonlinearity of the material on the micrometre scale. Such small features can be challenging to fabricate, and QPM is only practical in certain materials. When femtosecond pulses are used for nonlinear optics, achieving the best performance becomes increasingly challenging because, in addition to phase-velocity matching, group-velocity matching must also be maintained. Meeting these two conditions simultaneously is difficult and failing to do so results in limited conversion efficiency or temporal broadening of the ultrashort pulses.

To avoid the difficulties of directly fabricating QPM materials, it is possible to use laser light to generate self-organized nonlinear gratings (SONGs), which can provide QPM for nonlinear processes[5–8]. For example, in materials such as SiO_2, which do not normally exhibit a bulk quadratic nonlinearity ($\chi^{(2)}$), irradiation with a laser can form permanent electric fields in the material, which act on the material's cubic nonlinearity ($\chi^{(3)}$) to produce an effective quadratic nonlinearity $\chi^{(2)}_{\mathrm{eff}}$. Moreover, because this induced electric field is formed via the interference of the fundamental with its own second harmonic (Fig. 1a), the direction of the field automatically switches with the correct periodicity for the QPM of second-harmonic generation (SHG). Although this technique provides a simplified method for fabricating a nonlinear grating for SHG, the low $\chi^{(2)}_{\mathrm{eff}}$ of SONGs in SiO_2 has historically limited the total conversion efficiency. More recently, the SONG concept has been reinvigorated through the observation of photoinduced SHG in nanophotonic waveguides made from stoichiometric silicon nitride (Si_3N_4, hereafter SiN)[9,10], which offer strong spatial confinement of the light, scalable fabrication and an improved $\chi^{(2)}_{\mathrm{eff}}$. However, all previous implementations of photoinduced SHG (in both SiO_2 and SiN) were realized under conditions of strong group-velocity mismatch, limiting the phase-matching bandwidth, as well as the conversion efficiency for femtosecond pulses.

Here, we show that dispersion-engineered SiN photonic waveguides, which are currently enabling breakthroughs in ultrafast $\chi^{(3)}$ nonlinear optics[11–15], can also serve as a versatile platform for $\chi^{(2)}$ nonlinear optics with femtosecond pulses through the formation of SONGs. Leveraging the high effective index contrast of SiN waveguides (with air top-cladding)[12,16], we achieve group-velocity matching for SHG by engineering the waveguide cross-section. Under these conditions, the formation of a SONG proceeds on the timescale of a few tens of seconds and results in a QPM grating that supports the entire bandwidth of the femtosecond pulse with high conversion efficiency. Our model of photoinduced QPM is verified through the use of SHG microscopy to make the first direct observation of a SONG. Furthermore, we derive the equations that govern SONG formation for femtosecond pulses and confirm the crucial role of group-velocity matching. Finally, we demonstrate that a suitably prepared SiN waveguide can simultaneously generate light at the second-harmonic wavelength via $\chi^{(2)}$ and $\chi^{(3)}$ pathways, enabling f–$2f$ self-referencing

[1]Time and Frequency Division, National Institute of Standards and Technology, Boulder, CO, USA. [2]Department of Physics and Soft Materials Research Center, University of Colorado, Boulder, CO, USA. [3]Department of Electrical and Computer Engineering, Johns Hopkins University, Baltimore, MD, USA. [4]Microsystems and Nanotechnology Division, NIST, Gaithersburg, MD, USA. [5]Department of Electrical, Computer, and Energy Engineering, University of Colorado, Boulder, CO, USA. [6]Renewable and Sustainable Energy Institute, NREL and University of Colorado, Boulder, CO, USA. [7]Department of Physics, University of Colorado, Boulder, CO, USA. *e-mail: danhickstein@gmail.com; scott.papp@colorado.edu

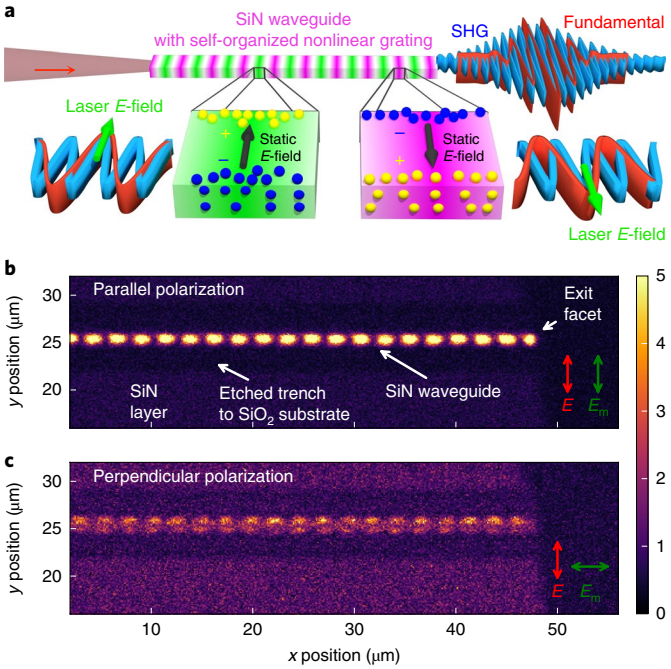

Fig. 1 | SONG formation in nanophotonic waveguide. a, The interference of fundamental and SHG light forces positive charges to one side of the waveguide and negative charges to the other, forming a static electric field, which enables an effective $\chi^{(2)}$. The phase walk-off between the two fields switches the direction of the electric field, automatically generating a self-organized nonlinear grating with the correct periodicity to provide quasi-phase-matching for the SHG process. The SONG produces stronger SHG, which, in turn, produces a stronger SONG, until saturation is reached. The geometry of the waveguide provides group-velocity matching, allowing for enhanced SHG conversion efficiency. **b**, An SHG microscopy image reveals the periodic modulation of the effective $\chi^{(2)}$. **c**, The same waveguide, probed with perpendicular polarization, reveals a double-lobed structure, confirming the charge localization. The arrows in **b** and **c** indicate the polarization directions of the preparation laser (E) and the microscopy laser (E_m).

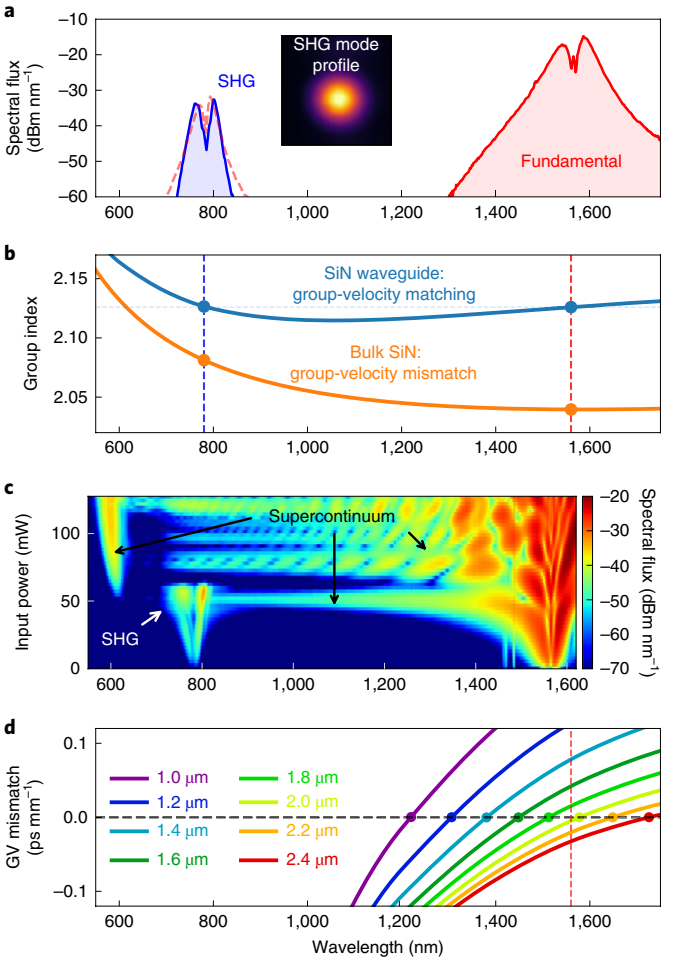

Fig. 2 | SHG in amorphous SiN waveguides using femtosecond pulses. **a**, Experimentally, femtosecond pulses at 1,560 nm generate second-harmonic light near 780 nm. The dashed red line shows the fundamental spectrum plotted at half the wavelength, demonstrating that the bandwidth is preserved. Inset: the second harmonic is generated into the fundamental quasi-transverse-electric (TE_{00}) mode. **b**, The group index of bulk SiN monotonically decreases with wavelength, preventing group-velocity matching for SHG. However, the group index of a 650×1,970 nm SiN waveguide provides perfect group-velocity matching for 1,560 nm SHG. **c**, SHG is favoured at relatively low input pulse intensities. At input powers over ~60 mW, supercontinuum generation takes place and no SHG is seen. **d**, The fundamental-mode wavelength where group-velocity (GV) matching with the second-harmonic is achieved increases with increasing waveguide width.

of a laser frequency comb. This represents the first f–$2f$ stabilization of a frequency comb using a single amorphous material and demonstrates how photonic waveguides can serve as an appealing platform for both $\chi^{(2)}$ and $\chi^{(3)}$ nonlinear optics with ultrafast sources.

Results and discussion

Photoinduced SHG. Our measurements involved coupling a pulsed laser into a SiN waveguide and measuring the output spectrum. We generated ~200 fs pulses using a compact Er:fibre laser with a centre wavelength of 1,560 nm and coupled ~400 pJ (40 mW at 100 MHz repetition rate) into various SiN waveguides[11,12]. The waveguides were made from SiN (deposited using low-pressure chemical vapour deposition, LPCVD) and had SiO_2 bottom cladding but air cladding on the top and sides, which allowed group-velocity dispersion profiles not achievable with typical full SiO_2 cladding.

After a build-up time of a few tens of seconds, we observed broadband SHG with ~1% total conversion efficiency (Fig. 2). Once the waveguide has been prepared in this way, the laser can be turned off, and the second-harmonic light reappears immediately upon turning the laser back on. However, if the laser power is increased above ~60 mW, the supercontinuum generation process[12,17] produces strong orange light (near 600 nm) and the SHG process is quickly quenched (Fig. 2c). Decreasing the power below 40 mW allows the second harmonic to build up once again. This behaviour indicates that the SHG results from the formation of a SONG[7,9,10].

As has been described for photoinduced SHG with long pulses[5–10], the gradual increase in SHG that we observe is a hallmark of the SONG formation process. According to this model, the process begins when a small intensity of second harmonic is generated, which may occur because of surface effects, a small static electric field or stress in the waveguide. This small intensity of the second harmonic interferes with the fundamental, creating an asymmetric field that forces positive charges to one side of the waveguide and negative charges to the other. Recent studies of SHG in SiN waveguides[9,10] have proposed that electrons and holes are the relevant charge carriers. The direction of charge separation depends on the phase between the fundamental and second harmonic. Because the two wavelengths typically have different refractive indices, the direction of charge separation switches along the waveguide as the phase slips between the two fields.

If the separated charges can be stabilized at trap sites or defects in the material, then the static electric field will induce a $\chi^{(2)}_{eff}$ in the material that oscillates sinusoidally along the waveguide length with the correct period to quasi-phase-match SHG. The generated second-harmonic light interferes with the fundamental to produce more charge separation, which, in turn, enables stronger SHG. This positive feedback continues until the process saturates.

Group-velocity matching. In contrast to previous studies of photoinduced SHG in SiN waveguides[9,10], which observed SHG in any waveguide, regardless of geometry, we only generate the second harmonic across a small range of waveguide widths. This difference is a result of group-velocity matching, with the strongest SHG appearing for waveguide widths that allow the fundamental and the second harmonic to travel with the same group velocity. Importantly, the SHG from our group-velocity-matched waveguides has an output mode that does not contain any nodes (Fig. 2a, inset), indicating that the second harmonic is generated in the fundamental quasi-transverse-electric (TE_{00}) mode. This is distinct from previous studies of SHG in SiN waveguides[9,10], which observe SHG in higher-order modes.

For any waveguide SONG, the formation involves a competition between various spatial modes (fundamental and higher order) of the waveguide to determine which second-harmonic mode will be favoured[9,10]. For pulses longer than a few picoseconds, higher-order modes can offer the lowest phase mismatch. Phase matching to higher-order modes is intrinsically narrowband due to the strong group-velocity walk-off between the fundamental and higher-order modes. Instead, if femtosecond pulses are used, the situation can be reversed, because the phase mismatch must be considered across the entire bandwidth of the pump. In the case of perfect group-velocity matching, every wavelength in the pump spectrum has the same phase mismatch for SHG (neglecting higher-order dispersion). Some of our waveguides achieve group-velocity matching for SHG to the fundamental mode and, consequently, our broad-bandwidth femtosecond pulses preferentially form a grating with the correct periodicity to provide QPM for SHG to the TE_{00} mode.

The wavelength where group-velocity matching for SHG occurs can be tuned simply by changing the waveguide dimensions (Fig. 2d). In our case, a waveguide with 2,000 nm width offers the lowest group-velocity mismatch at the 1,560 nm centre wavelength of our laser. However, because we have a broadband pump, we find that we can generate SHG from waveguides with widths between 1,900 and 2,300 nm. As the width is increased, the peak of the second harmonic moves to longer wavelengths, in agreement with the trend in the group-velocity matching (Fig. 2d and Supplementary Figs. 1 and 2).

The SONG can persist indefinitely and, once prepared, it can be used for nonlinear optics with other laser sources. We use this capability to directly map the phase-matching bandwidth of the gratings by using a few-milliwatt continuous-wave (c.w.) laser for SHG with each waveguide (Supplementary Fig. 3). By tuning the c.w. laser from 1,520 to 1,620 nm, we observe a broad phase-matching bandwidth, in some cases spanning 60 nm, confirming that group-velocity matching has been achieved. Additionally, as expected from Fig. 2d, the peak conversion efficiency moves to longer wavelengths with increasing waveguide width. Thus, the group-velocity-matching condition provides advantages for both femtosecond pulses and tunable c.w. light.

Microscopy of self-organized nonlinear gratings. To confirm the presence of periodic $\chi^{(2)}$ gratings in our waveguides, we first prepare the SONGs by irradiating each waveguide for ~10 min. We then employ a SHG microscope (see Methods) to record the first direct images of a SONG. Although the periodic grating is created by propagating 1,560 nm pulses along the waveguide (from left to right in Fig. 1b,c), the microscope probes the sample from top to bottom with 870 nm pulses. The intensity of the emitted second-harmonic light is measured, and the laser is raster-scanned across the chip to form a two-dimensional image of the waveguide and the surrounding material. Although most of the SiN material appears dark, the waveguides that exhibit SHG appear bright as a result of the strong induced $\chi^{(2)}_{eff}$ (Fig. 1b,c and Supplementary Fig. 4). The observed periodicity of the SONG matches the period expected for QPM of 1,560 nm SHG (Supplementary Fig. 5). None of the SONGs exhibit any significant change in period along the length, confirming that group-velocity matching—not variations in the grating period—is responsible for the broad-bandwidth SHG (Supplementary Fig. 6). Our results are in general agreement with what has been observed when SONGs in SiO_2 were visualized using electric-field-sensitive etching techniques[18].

To further characterize the SONG, we recorded numerous SHG microscopy images along the length of several waveguides and fitted a sinusoidal function to the integrated SHG intensity in each image (Supplementary Fig. 6). We found that the envelope of the sinusoidal SONG follows a sigmoid function, where the SONG is not observable at the entrance facet, rapidly increases at some point along the waveguide length, and then reaches a constant value that is maintained until the exit facet. This behaviour suggests that the SONG reaches a saturation condition, where the fundamental and SHG can no longer increase the intensity of the SONG. The origin of this saturation is not clear, though several possibilities exist that are related to the properties and sensitivities of the SiN defect sites present in the material. Future experiments that examine that nature of the saturation along with systematic variation of the material properties such as stoichiometry may provide insight into how $\chi^{(2)}_{eff}$ can be increased.

Conversion efficiency. For some waveguides, the SHG conversion exceeds 0.005% per watt of peak power (Supplementary Fig. 3), which is an excellent conversion efficiency for a device that provides SHG across such a large bandwidth. As we know the approximate length of the grating from the microscopy experiments, we can use equations (9) and (10) from ref. [10] to estimate the $\chi^{(2)}_{eff}$ to be 0.5 pm V^{-1} for the 2,100 nm waveguide. It is likely that the lengths of the SONGs that we observe are limited by the broad bandwidth of our laser pulses, and that much longer gratings could be produced if narrower-bandwidth pulses propagated through longer waveguides. A longer grating would provide a narrower phase-matching bandwidth, but enhanced conversion efficiency.

Using our calculated $\chi^{(2)}_{eff}$ we can make a comparison to a periodically poled lithium niobate (PPLN) waveguide with $\chi^{(2)} = 25$ pm V^{-1} and an effective mode area of 100 μm^2. To our knowledge, such PPLN waveguides are the most efficient commercial off-the-shelf SHG devices. Figure 3a shows the maximum conversion efficiency achievable, while preserving the full bandwidth of the pulse. As the pulse duration becomes longer, a group-velocity-matched device can support a longer grating and can therefore provide higher conversion efficiency. Given the optimal length for both devices, a SiN waveguide should outperform a PPLN waveguide for pulse durations longer than ~30 fs.

Of course, increasing the length of the waveguide requires that the waveguide loss is low. Fortunately, recent efforts have realized SiN waveguides with losses on the order of 1 dB m^{-1} (ref. [13]) and suggest that the losses may be decreased orders of magnitude further before reaching the material limit. Second, increasing the length of the waveguide while preserving the bandwidth of the SHG requires that the waveguide offers low phase mismatch over the entire bandwidth of the input pulse. This amounts to a waveguide that exhibits low and flat group velocity dispersion (GVD) over a broad spectral region. Fortunately, nanophotonic waveguides provide exceptional control over GVD, and several studies[19,20] have shown that

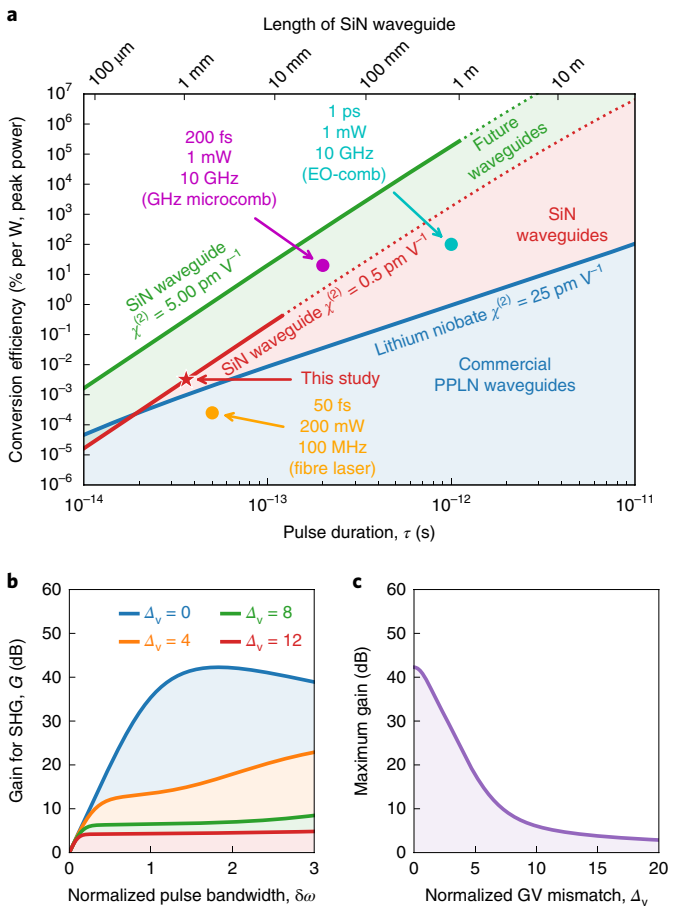

Fig. 3 | Theoretical estimate of SHG with SiN waveguides. a, Using the $\chi^{(2)}_{\mathrm{eff}}$ obtained in this study and the calculated dispersion of a SiN waveguide that offers group-velocity matching, we plot the conversion efficiency of SiN waveguides (red line) as a function of the pulse duration (τ). The green line represents the performance if $\chi^{(2)}_{\mathrm{eff}}$ is increased by a factor of 10. In comparison to a commercial waveguide made from PPLN (blue), the SiN waveguides provide a τ^4 scaling of the conversion efficiency rather than the τ^2 scaling of a group-velocity-mismatched material. Filled circles represent the per W conversion efficiency required to achieve 10% conversion for various laser systems. **b**, Gain for SHG versus the input pulse bandwidth $\delta\omega$ for various values of the normalized group-velocity mismatch Δ_v. In general, better group-velocity matching provides better SHG conversion. **c**, For photoinduced SHG with femtosecond pulses, the highest conversion efficiency will be realized through perfect group-velocity matching.

'slot waveguide' geometries can be used to provide ultraflat GVD profiles. Moreover, if the GVD at the pump wavelength can be normal dispersion, the supercontinuum process seen in Fig. 2 can be avoided, which would allow higher peak powers to be used. Higher average powers could also be used, as similar SiN waveguides have demonstrated stable operation at several watts of average power[21,22].

If the $\chi^{(2)}_{\mathrm{eff}}$ could be further increased (green line, Fig. 3a), SONGs based on SiN could enable SHG with even lower pulse energies, possibly enabling useful frequency conversion of unamplified electro-optic[21] and microresonator-based[23] frequency combs (filled circles, Fig. 3a). In the future, $\chi^{(2)}_{\mathrm{eff}}$ could be optimized via several methods including engineering the material to support higher electric fields, finding a material that has a stronger $\chi^{(2)}_{\mathrm{eff}}$ response via slight rearrangement of the atomic positions or selecting a material with higher $\chi^{(3)}$. As an example of how a high $\chi^{(3)}$ can result in a high $\chi^{(2)}_{\mathrm{eff}}$, a recent study[24] showed that silicon, a material with a strong $\chi^{(3)}$, can be biased with electrodes to enable a $\chi^{(2)}_{\mathrm{eff}}$ of 41 pm V^{-1}.

Analytical description of grating formation. Although several models exist for photoinduced grating formation in the case of c.w. light[7,25,26], to our knowledge, no theoretical treatment has been attempted for femtosecond pulses. Thus, we explore the photoinduced grating formation process analytically, expanding on the approach of Anderson and co-workers[7] (the complete analysis is presented in Supplementary Section 2). In brief, by assuming that we can model the total photoinduced grating as a coherent sum of contributions from all of the individual frequencies, we find that the second-harmonic pulse energy increases from the quantum noise level at the input $U_2(0)$ to the output value of $U_{2,\mathrm{out}} = U_2(0)\exp(G)$, with the total logarithmic gain for SHG given by

$$G(\delta\omega, \Delta_v) \sim G_0 \delta\omega \int_0^1 \frac{\exp\left(\frac{-(\Delta_v \delta\omega z')^2}{2(1+\delta\omega^4 z'^2)}\right)}{\sqrt{1+\delta\omega^4 z'^2}} \mathrm{d}z' \quad (1)$$

where $\delta\omega = \Delta\omega\sqrt{\delta\beta L}$ is the normalized pulse bandwidth, $\Delta\omega$ is the pulse bandwidth, L is the length of the waveguide, $\delta\beta = \beta_{2\omega_0} - \beta_{\omega_0}$ is the difference in GVD at the fundamental and second-harmonic frequencies, and $\Delta_v = \delta v_g^{-1}\sqrt{L/\delta\beta}$ is the normalized group-velocity mismatch, where $\delta v_g^{-1} = v_{g,2\omega_0}^{-1} - v_{g,\omega_0}^{-1}$ is the (inverse) group-velocity mismatch between the fundamental and the SHG. The coefficient G_0 incorporates several material characteristics, including the effective coherent photoinjection coefficient, third-order nonlinear susceptibility, momentum scattering and recombination times, trapping cross-section and the effective cross-section of the waveguide, which makes a theoretical estimate of G_0 difficult. However, comparing our results with those of ref. [7], it is not unreasonable to assume that our gain is similar, that is, on the order of 40 dB.

Equation (1) indicates that better group-velocity matching (lower Δ_v) allows for larger maximum gain. Better group-velocity matching also allows for SHG with shorter pulses, explaining why previous studies observed SHG with picosecond pulses and how the group-velocity matching enabled by nanophotonic waveguides allows SHG with femtosecond pulses (Fig. 3b,c). Moreover, in Supplementary Section 3, we provide a theory that describes the time-dependent evolution of the SONG in the presence of saturation effects.

Simplified frequency-comb stabilization. A particular advantage of these SiN nanophotonic waveguides is that they exhibit simultaneous supercontinuum generation (a $\chi^{(3)}$ process) and SHG ($\chi^{(2)}$), which allows for f–$2f$ self-referencing of laser frequency combs. In previous experiments[27], waveguides made from aluminium nitride, a material with bulk $\chi^{(3)}$ and $\chi^{(2)}$, provided both SHG and supercontinuum generation and allowed for a simplified scheme for self-referencing. However, nanojoule pulse energies were required, because SHG to the fundamental mode was strongly phase-mismatched and was consequently very dim. In contrast, in the case of SiN SONGs, the SHG is fully quasi-phase-matched and the conversion efficiency is much higher, which allows lower pulse energies to be used. For production of both SHG and supercontinuum at 780 nm, the pulse energy must be set appropriately. If it is too low, then insufficient supercontinuum is generated; if it is too high, then the SHG intensity is diminished. Fortunately, a regime exists where both supercontinuum and SHG are generated with sufficient intensity to detect the carrier-envelope-offset frequency (f_{ceo}) with ~30 dB signal-to-noise ratio (Fig. 4). We stabilize f_{ceo} by feeding back to the laser current. By counting the in-loop beat note with a frequency counter, we verify that the stabilization performance is equivalent to a traditional f–$2f$ interferometer[12].

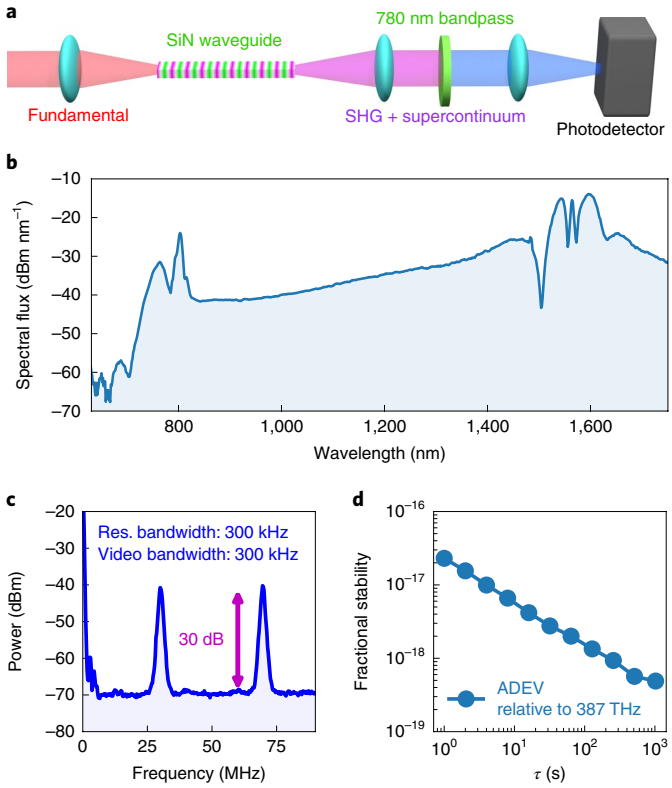

Fig. 4 | Frequency comb stabilization through one-step *f*–2*f* self-referencing. a, In contrast to a typical *f*–2*f* self-referencing experiment, which requires separate SHG and supercontinuum generation media, a single SiN waveguide provides both *f* and 2*f* light, which can be selected using a simple filter and detected with a silicon photodetector. **b**, The input power is set at a level that provides both supercontinuum and second-harmonic light near 800 nm. **c**, The carrier-envelope offset frequency (f_{ceo}) is detected with 30 dB signal-to-noise ratio, which is sufficient for stabilizing the frequency comb without phase slips. **d**, The Allan deviation of the locked f_{ceo} (recorded with a separate photodetector and frequency counter) confirms that f_{ceo} has been stabilized to a level suitable for precision measurements.

Microsopic mechanism of SONG formation. SiN is known to provide a high density of trap sites, which may hold electrons for more than 100 years[28], making SiN an appealing material for non-volatile computer memory[29]. Although the precise microscopic mechanism for charge trapping in our LPCVD SiN waveguides is not known with absolute certainty, numerous previous studies suggests that Si dangling bonds may be responsible. Indeed, a series of electron-spin-resonance measurements[30–34] have identified Si dangling bonds as the dominant trap site. Moreover, it is known that Si nanocrystals can form in the growth of SiN films, for example if the conditions deviate from the stoichiometric point towards Si-rich films[35] or during post-growth annealing of stoichiometric nitride films[36,37]. Additionally, LPCVD SiN has been has been shown to provide a higher density of trap sites than SiN deposited via plasma-enhanced CVD[38]. Overall, we expect SiN stoichiometry and deposition conditions to be key parameters for future studies that improve trapped charge[39].

Consistent with previous descriptions of SONG formation via trap sites in SiN[9,10], we find that the generation of visible-wavelength photons through the supercontinuum generation process can lead to suppression of the SHG process, presumably by promoting trapped electrons to the conduction band and erasing the SONG. Similarly, an ultraviolet lamp focused on top of the waveguide can also lead to erasure (see Methods). Indeed, Si dangling bonds in SiN have a noted sensitivity to short-wavelength light[30], solidifying the connection between these defects and SONGs. Moreover, measurements of photoluminescence have further clarified the optical properties of the defects[35,39], indicating that they may be candidates for the photosensitive behaviour that we observe. Thus, while it is not possible to identify the trap sites with certainty, the available evidence points to Si dangling bonds and suggests that increasing the density of such defects may enable better nonlinear optical performance in SONG-based devices.

Conclusion

We have shown that nanophotonic waveguides can provide QPM for nonlinear processes via self-organized nonlinear grating formation. Unlike previous observations of such gratings, we form the gratings using femtosecond pulses and observe broadband SHG to the fundamental mode of the waveguide. These nanophotonic waveguides provide both quasi-phase matching and group-velocity matching for SHG, opening the door for dispersion-engineered $\chi^{(2)}$ ultrafast nonlinear optics in amorphous waveguides. Using SHG microscopy, we record direct images of self-organized nonlinear gratings. Additionally, by analytically deriving the equations that govern the formation of the nonlinear gratings, we quantify the role of group velocity and GVD mismatch in the self-organization process. Finally, we demonstrate the utility of such nanophotonic waveguides by self-referencing a laser frequency comb with a single waveguide. In the future, longer and more nonlinear waveguides would enable high-efficiency nonlinear optics in situations previously considered impossible.

Online content

Any methods, additional references, Nature Research reporting summaries, source data, statements of code and data availability and associated accession codes are available at https://doi.org/10.1038/s41566-019-0449-8.

Received: 31 August 2018; Accepted: 28 April 2019;
Published online: 3 June 2019

References

1. New, G. *Introduction to Nonlinear Optics* (Cambridge University Press, 2011).
2. Schneider, T. *Nonlinear Optics in Telecommunications* (Springer, 2004).
3. Weston, M. M. et al. Efficient and pure femtosecond-pulse-length source of polarization-entangled photons. *Opt. Express* **24**, 10869–10879 (2016).
4. Garmire, E. Nonlinear optics in daily life. *Opt. Express* **21**, 30532–30544 (2013).
5. Dianov, E. & Starodubov, D. Photoinduced second-harmonic generation in glasses and glass optical fibers. *Opt. Fiber Technol.* **1**, 3 (1994).
6. Balakirev, M. K., Vostrikova, L. I. & Smirnov, V. A. Photoelectric instability in oxide glass. *JETP Lett.* **66**, 809–815 (1997).
7. Anderson, D. Z., Mizrahi, V. & Sipe, J. E. Model for second-harmonic generation in glass optical fibers based on asymmetric photoelectron emission from defect sites. *Opt. Lett.* **16**, 796 (1991).
8. Stolen, R. H. & Tom, H. W. K. Self-organized phase-matched harmonic generation in optical fibers. *Opt. Lett.* **12**, 585 (1987).
9. Billat, A. et al. Large second harmonic generation enhancement in Si_3N_4 waveguides by all-optically induced quasi-phase-matching. *Nat. Commun.* **8**, 1016 (2017).
10. Porcel, M. A. G. et al. Photo-induced second-order nonlinearity in stoichiometric silicon nitride waveguides. *Opt. Express* **25**, 33143 (2017).
11. Carlson, D. R. et al. Photonic-chip supercontinuum with tailored spectra for counting optical frequencies. *Phys. Rev. Appl.* **8**, 014027 (2017).
12. Carlson, D. R. et al. Self-referenced frequency combs using high-efficiency silicon-nitride waveguides. *Opt. Lett.* **42**, 2314–2317 (2017).
13. Ji, X. et al. Ultra-low-loss on-chip resonators with sub-milliwatt parametric oscillation threshold. *Optica* **4**, 619 (2017).
14. Mayer, A. S. et al. Frequency comb offset detection using supercontinuum generation in silicon nitride waveguides. *Opt. Express* **23**, 15440–15451 (2015).
15. Porcel, M. A. G. et al. Two-octave spanning supercontinuum generation in stoichiometric silicon nitride waveguides pumped at telecom wavelengths. *Opt. Express* **25**, 1542–1554 (2017).
16. Briles, T. C. et al. Interlocking Kerr-microresonator frequency combs for microwave to optical synthesis. *Opt. Lett.* **43**, 2933 (2018).
17. Dudley, J. M., Genty, G. & Coen, S. Supercontinuum generation in photonic crystal fiber. *Rev. Mod. Phys.* **78**, 1135 (2006).

18. Margulis, W., Laurell, F. & Lesche, B. Imaging the nonlinear grating in frequency-doubling fibres. *Nature* **378**, 699–701 (1995).
19. Zhu, M. et al. Ultrabroadband flat dispersion tailoring of dual-slot silicon waveguides. *Opt. Express* **20**, 15899–15907 (2012).
20. Zhang, L., Yue, Y., Beausoleil, R. G. & Willner, A. E. Flattened dispersion in silicon slot waveguides. *Opt. Express* **18**, 20529–20534 (2010).
21. Carlson, D. R. et al. Ultrafast electro-optic light with subcycle control. *Science* **361**, 1358–1363 (2018).
22. Metcalf, A. J. et al. Stellar spectroscopy in the near-infrared with a laser frequency comb. *Optica* **6**, 233–239 (2019).
23. Lamb, E. S. et al. Optical-frequency measurements with a Kerr microcomb and photonic-chip supercontinuum. *Phys. Rev. Appl.* **9**, 024030 (2018).
24. Timurdogan, E., Poulton, C. V., Byrd, M. J. & Watts, M. R. Electric field-induced second-order nonlinear optical effects in silicon waveguides. *Nat. Photon.* **11**, 200–206 (2017).
25. Zel'dovich, B. Y. & Chudinov, A. N. Interference of fields with frequencies ω and 2ω in external photoelectric effect. *JETP Lett.* **50**, 439–441 (1989).
26. Baranova, N., Chudinov, A. & Zel'dovich, B. Polar asymmetry of photoionization by a field with $<E^3> \neq 0$. Theory and experiment. *Opt. Commun.* **79**, 116 (1990).
27. Hickstein, D. D. et al. Ultrabroadband supercontinuum generation and frequency-comb stabilization using on-chip waveguides with both cubic and quadratic nonlinearities. *Phys. Rev. Appl.* **8**, 014025 (2017).
28. Tzeng, S.-D. & Gwo, S. Charge trapping properties at silicon nitride/silicon oxide interface studied by variable-temperature electrostatic force microscopy. *J. Appl. Phys.* **100**, 023711 (2006).
29. Fujita, S. & Sasaki, A. Dangling bonds in memory-quality silicon nitride films. *J. Electrochem. Soc.* **132**, 398–402 (1985).
30. Krick, D. T., Lenahan, P. M. & Kanicki, J. Nature of the dominant deep trap in amorphous silicon nitride. *Phys. Rev. B* **38**, 8226–8229 (1988).
31. Warren, W. L. & Lenahan, P. M. Electron-nuclear double-resonance and electron-spin-resonance study of silicon dangling-bond centers in silicon nitride. *Phys. Rev. B* **42**, 1773–1780 (1990).
32. Lenahan, P. M. & Curry, S. E. First observation of the ^{29}Si hyperfine spectra of silicon dangling bond centers in silicon nitride. *Appl. Phys. Lett.* **56**, 157–159 (1990).
33. Warren, W. L., Lenahan, P. M. & Curry, S. E. First observation of paramagnetic nitrogen dangling-bond centers in silicon nitride. *Phys. Rev. Lett.* **65**, 207–210 (1990).
34. Warren, W. L., Rong, F. C., Poindexter, E. H., Gerardi, G. J. & Kanicki, J. Structural identification of the silicon and nitrogen dangling-bond centers in amorphous silicon nitride. *J. Appl. Phys.* **70**, 346–354 (1991).
35. Wang, M., Li, D., Yuan, Z., Yang, D. & Que, D. Photoluminescence of Si-rich silicon nitride: defect-related states and silicon nanoclusters. *Appl. Phys. Lett.* **90**, 131903 (2007).
36. Seol, K. S., Futami, T., Watanabe, T., Ohki, Y. & Takiyama, M. Effects of ion implantation and thermal annealing on the photoluminescence in amorphous silicon nitride. *J. Appl. Phys.* **85**, 6746–6750 (1999).
37. Hafsi, N., Bouridah, H., Beghoul, M. R. & Haoues, H. Photoluminescence from silicon nanocrystals embedded in silicon nitride fabricated by low-pressure chemical vapor deposition followed by high-temperature annealing. *J. Appl. Phys.* **117**, 063105 (2015).
38. Park, Y. C., Jackson, W. B., Johnson, N. M. & Hagstrom, S. B. Spatial profiling of electron traps in silicon nitride thin films. *J. Appl. Phys.* **68**, 5212 (1990).
39. Gritsenko, V. et al. Silicon dots/clusters in silicon nitride: photoluminescence and electron spin resonance. *Thin Solid Films* **353**, 20–24 (1999).

Acknowledgements

The authors thank G. Moille, N. Sanford and the National Institute of Standards and Technology (NIST) Boulder Editorial Review Board for providing helpful feedback on this manuscript, and K. Dorney, J. Ellis, H. Kapteyn and M. Murnane for the timely loan of a polarizer. This work is supported by AFOSR under award no. FA9550-16-1-0016, DARPA (DODOS and ACES programmes), NIST and NRC. Nonlinear optical imaging instrumentation at CU-Boulder was supported by the National Science Foundation Grant DMR-1420736. Certain commercial equipment, instruments or materials are identified here in order to specify the experimental procedure adequately. Such identification is not intended to imply recommendation or endorsement by NIST, nor is it intended to imply that the materials or equipment identified are necessarily the best available for the purpose.

Author contributions

D.D.H. and D.R.C. conducted the SHG experiments. D.D.H., H.M. and I.I.S. conceived and conducted the microscopy experiment. K.S. and D.W. designed, fabricated and characterized the SiN waveguides. D.D.H., D.R.C., S.B.P., S.A.D. and A.K. analysed and interpreted the data. J.B.K. developed the theoretical models.

Competing interests

D.D.H. is currently employed by KMLabs, Inc., a company that manufactures femtosecond lasers. D.R.C. is an owner of Octave Photonics, a company specializing in nonlinear nanophotonics.

Additional information

Supplementary information is available for this paper at https://doi.org/10.1038/s41566-019-0449-8.

Reprints and permissions information is available at www.nature.com/reprints.

Correspondence and requests for materials should be addressed to D.D.H. or S.B.P.

Publisher's note: Springer Nature remains neutral with regard to jurisdictional claims in published maps and institutional affiliations.

Methods

Waveguide design and fabrication. The SiN waveguides[11] had the following physical dimensions: 12 mm length, 650 nm height and a width that was varied in the experiments (as indicated throughout the Article). The physical dimensions were constant along the length. All of the waveguides were supported from underneath by a 3 μm SiO_2 cladding, and the sides and top were exposed to air. To fabricate the devices we began with a thermally oxidized Si wafer and used LPCVD of SiN at a temperature of 800 °C, pressure of 250 mtorr and a gas mixture of dichlorosilane and ammonia in a 1:3 ratio. The process was optimized in our deposition system for stoichiometric SiN growth, resulting in low-optical-loss films following all our processing. Grown films were characterized by stress measurements and spectroscopic ellipsometry, and exhibited parameters consistent with those widely observed for stoichiometric SiN. We then used electron-beam lithography to define the waveguide geometries, and the waveguide pattern was transferred to the SiN film using CHF_3 reactive-ion etching. Following typical cleaning procedures to remove remnant resist, the wafer was thermally annealed at 1,100 °C for 3 h in a nitrogen environment at atmospheric pressure to limit the influence of Si–H and N–H bond absorption resonances in the telecom band. Finally, we cleaved the wafer by hand into three chips, which we used in our experiments. The waveguide modes (and their effective indices) were calculated using a vector finite-difference modesolver[40,41] using published refractive indices for Si_3N_4 (ref. [42]) and SiO_2 (ref. [43]).

SHG. SHG experiments were completed at NIST in Boulder, Colorado. We generate the second harmonic by coupling 1,560 nm light from a compact 100 MHz Er-fibre frequency comb[44] into each SiN waveguide. The power was adjusted using a computer-controlled-rotation mount containing a half-waveplate, which was placed before a polarizer. The polarization was set to horizontal (along the long dimension of the rectangular waveguide) and excited the lowest-order TE_{00} mode of the waveguide.

Interestingly, in some cases we observed strong temporal oscillations in the intensity of the second harmonic. Similar oscillations have also been observed in other studies of SiN waveguides[9,10]. In our waveguides, the oscillations typically became faster when the laser intensity increased (Supplementary Fig. 7). Additionally, they were nearly absent for waveguides that exhibited the best group-velocity matching, suggesting that they are related the the group-velocity matching conditions. We suspect that these oscillations result from slight changes in the period of the grating during the formation process. For example, an initial grating might form with a period that phase-matches SHG at the peak of the pump spectrum. Over time, the grating may slightly change period to provide phase-matching for the wavelength that experiences the best group-velocity matching in the waveguide.

Frequency-comb stabilization. We used the SiN waveguides to provide a simplified, low-power method to stabilize our Er-fibre frequency comb. By setting the power level to ~40 mW we generated light near 780 nm via both SHG (a $\chi^{(2)}$ process) and supercontinuum generation (a $\chi^{(3)}$ process). The interference of these two pathways allows f_{ceo} to be detected simply by detecting the light near 780 nm. This approach offers an alternative to conventional f–$2f$ self-referencing, which separately generates the supercontinuum light in one material and the second harmonic light in another material[12].

The light emitted by the waveguide was collimated with a microscope objective with a numerical aperture (NA) of 0.85 (Newport M60x) and filtered with a 780 nm bandpass filter (Thorlabs FB-780-10). A beamsplitter directed the light to two separate silicon avalanche photodiodes (APDs, Thorlabs APD430A and APD210). The electrical signal from the first photodiode was connected to a Red Pitaya field-programmable gate array (FPGA) board running the 'Frequency comb digital-phase-locked-loop' firmware[44,45], which was used to feedback to the oscillator pump diode current in order to stabilize f_{ceo}. The electrical signal for the second APD was connected to a Λ-type frequency counter, which provided an 'electrical out-of-loop' confirmation of the f_{ceo} stabilization.

SHG microscopy. After the SONGs were prepared at NIST, the waveguides were transported to the University of Colorado where SHG microscopy experiments were completed at the Smalyukh Lab. The ability for the SONGs to persist after being transported several kilometres demonstrates that they are robust to typical vibration, shock and temperature changes. To obtain the SHG microscopy images, a Ti:sapphire laser (Coherent Chameleon Ultra II) was used to generate 140 fs pulses with a central wavelength of 870 nm at an 80 MHz repetition rate. The laser was attenuated so that, at the sample, the average power was 6 mW, corresponding to a pulse energy of 75 pJ. The beam entered an inverted microscope system (Olympus IX81) and was focused onto the sample using an Olympus UPlanFLN ×40 objective with NA = 0.75, providing a peak intensity of ~4.7×10^{10} W cm^{-2}, assuming a diffraction-limited spot size. The focused spot was raster-scanned across the sample using a galvo mirror system (Olympus Fluorview FV300). The reflected second-harmonic light propagated back into the galvo-mirror system where it was collected with a photomultiplier tube. Images were collected at a rate of ~32,000 pixels s^{-1} and a size of 512 × 512 pixels, for an image acquisition rate of ~9 s per image. The images were averaged using a 10-frame Kalman filter, for a total acquisition time of ~90 s per averaged image.

Generally, the SHG microscopy experiment did not significantly alter the SONGs, indicating that it may be possible to record such images in situ, while the SONG is forming. However, in several cases, when the laser was left to raster over a small region for many minutes, we noticed a slow decrease in the intensity of the SHG being emitted from the waveguide, indicating that the SONG was being erased. It is not clear if the erasure is caused by the high peak intensity of the femtosecond pulses, the generated second harmonic or simply the average power. Additionally, during an initial microscopy attempt, we aligned the microscope by illuminating the chip with a 100 W mercury-vapour lamp (Olympus U-LH100HG), which emits high-power visible and ultraviolet light. However, we found that the focused light from this lamp appeared to rapidly erase the SONGs. On the other hand, we found that illumination with a lower-power halogen lamp (Olympus LG-PS2-5), which produces much lower levels of ultraviolet light, allowed the microscope to be aligned without affecting the observed SHG. Thus, we conclude that irradiation with high-energy photons is an effective method for grating erasure.

Estimation of the effective quadratic nonlinearity. Using a c.w. laser, we could generate the second harmonic from waveguides that had been suitably prepared by the femtosecond-pulsed laser. Because the c.w. laser does not experience significant spectral broadening as it propagates along the waveguide, it allows an accurate measurement of the SHG conversion efficiency. Additionally, because the SHG microscopy experiment provides estimates of the length of the grating in each waveguide, we could estimate the effective quadratic nonlinearity of our SiN waveguides. According to equation (5.37) of Weiner[46] and equation (3.19) of Suhara and Fujimura[47], we can write the conversion efficiency for SHG as

$$\frac{\eta}{P_\omega} = \frac{L^2 d_{\mathrm{eff}}^2}{S_{\mathrm{eff}}}\left(\frac{2\omega_0^2}{\varepsilon_0 c^3 n^3}\right) \tag{2}$$

where η is the conversion efficiency, P_ω is the peak power of the fundamental, L is the medium length, ε_0 is the permittivity of free space, ω_0 is the frequency of the fundamental, c is the speed of light, n is the index of the fundamental, S_{eff} is the effective mode area and the nonlinearity $d_{\mathrm{eff}} = 1/2\chi^{(2)}_{\mathrm{eff}}$.

We can see from equation (2) that increasing the medium length is equally important as increasing d_{eff}. Rearranging equation (2) to solve for d_{eff} yields

$$d_{\mathrm{eff}} = \sqrt{\left(\frac{\eta}{P_\omega}\right)\left(\frac{S_{\mathrm{eff}}}{L^2}\right)\left(\frac{\varepsilon_0 c^3 n^3}{2\omega_0^2}\right)} \tag{3}$$

Using a numerical vector finite-difference modesolver[40,41], we calculated that the effective area for 1,560 nm SHG in a 650 × 2,100 nm waveguide is 1.20 μm^2. Using the observed grating length (1.05 mm) and the observed conversion efficiency (0.0025% per W), we can use equation (3) to calculate $d_{\mathrm{eff}} = 0.25$ pm V^{-1} ($\chi^{(2)} = 0.5$ pm V^{-1}). This is in rough agreement with the value of $\chi^{(2)} = 0.3$ pm V^{-1} reported by Billat and others[9].

Data availability

The data that support the plots within this paper and other findings of this study are available from the corresponding authors upon reasonable request.

References

40. Fallahkhair, A. B., Li, K. S. & Murphy, T. E. Vector finite difference modesolver for anisotropic dielectric waveguides. *J. Lightwave Technol.* **26**, 1423–1431 (2008).
41. Bolla, L. *Empy: Electromagnetic Python* https://github.com/lbolla/EMpy (2017).
42. Luke, K., Okawachi, Y., Lamont, M. R. E., Gaeta, A. L. & Lipson, M. Broadband mid-infrared frequency comb generation in a Si_3N_4 microresonator. *Opt. Lett.* **40**, 4823–4826 (2015).
43. Malitson, I. H. Interspecimen comparison of the refractive index of fused silica. *J. Opt. Soc. Am.* **55**, 1205–1209 (1965).
44. Sinclair, L. C. et al. Invited article: a compact optically coherent fiber frequency comb. *Rev. Sci. Instrum.* **86**, 081301 (2015).
45. Tourigny-Plante, A. et al. An open and flexible digital phase-locked loop for optical metrology. *Rev. Sci. Instrum.* **89**, 093103 (2018).
46. Weiner, A. *Ultrafast Optics* (Wiley, 2009).
47. Suhara, T. & Fujimura, M. *Waveguide Nonlinear-Optic Devices* (Wiley, 2003).